RSC Advances

PAPER

View Article Online
View Journal | View Issue

Cite this: *RSC Adv.*, 2019, **9**, 10371

Hydrodesulfurization of dibenzothiophene using Pd-promoted Co–Mo/Al_2O_3 and Ni–Mo/Al_2O_3 catalysts coupled with ionic liquids at ambient operating conditions†

Yaseen Muhammad,[ab] Ata Ur Rahman,[b] Haroon Ur Rashid,[a] Maria Sahibzada,[c] Sidra Subhan[ab] and Zhangfa Tong *[a]

Sulfur compounds in fuel oils are a major source of atmospheric pollution. This study is focused on the hydrodesulfurization (HDS) of dibenzothiophene (DBT) *via* the coupled application of 0.5 wt% Pd-loaded Co–Mo/Al_2O_3 and Ni–Mo/Al_2O_3 catalysts with ionic liquids (ILs) at ambient temperature (120 °C) and pressure (1 MPa H_2). The enhanced HDS activity of the solid catalysts coupled with [BMIM]BF_4, $[(CH_3)_4N]Cl$, [EMIM]$AlCl_4$, and $[(n\text{-}C_8H_{17})(C_4H_9)_3P]Br$ was credited to the synergism between hydrogenation by the former and extractive desulfurization and better H_2 transport by the latter, which was confirmed by DFT simulation. The Pd-loaded catalysts ranked highest by activity *i.e.* Pd–Ni–Mo/Al_2O_3 > Pd–Co–Mo/Al_2O_3 > Ni–Mo/Al_2O_3 > Co–Mo/Al_2O_3. With mild experimental conditions of 1 MPa H_2 pressure and 120 °C temperature and an oil : IL ratio of 10 : 3.3, DBT conversion was enhanced from 21% (by blank Ni–Mo/Al_2O_3) to 70% by Pd–Ni–Mo/Al_2O_3 coupled with $[(n\text{-}C_8H_{17})(C_4H_9)_3P]Br$. The interaction of polarizable delocalized bonds (in DBT) and van der Waals forces influenced the higher solubility in ILs and hence led to higher DBT conversion. The IL was recycled four times with minimal loss of activity. Fresh and spent catalysts were characterized by FESEM, ICP-MS, EDX, XRD, XPS and BET surface area techniques. GC-MS analysis revealed biphenyl as the major HDS product. This study presents a considerable advance to the classical HDS processes in terms of mild operating conditions, cost-effectiveness, and simplified mechanization, and hence can be envisaged as an alternative approach for fuel oil processing.

Received 5th January 2019
Accepted 20th March 2019

DOI: 10.1039/c9ra00095j

rsc.li/rsc-advances

1. Introduction

Organosulfur compounds leading to the production of deleterious and hazardous sulfur oxides, *i.e.* SO_x, from the combustion of fuel oils has led to the permissible limits of sulfur becoming much more stringent over the years.[1] Among the many desulfurization approaches, such as oxidative desulfurization,[2] biodesulfurization[3] and extractive desulfurization,[4] hydrodesulfurization (HDS) ranks higher, attributed to its diverse nature, high practicability and efficiency.[5] HDS generally utilizes a Co or Ni sulfide phase added to Mo impregnated over Al_2O_3-supported catalysts.[6–8] Furthermore, incorporation of a third promoter metal, *i.e.* Pt, Pd, and Ir, can further enhance the HDS activity of classical catalysts.[5,9,10] Despite its efficient and versatile nature, HDS suffers from complex mechanization, poor safety and harsh temperature (380–400 °C) and pressure (8 MPa) operating conditions.[11–13] Similarly, expensive catalytic promoters like Pt, Pd, and Ir further add to the uncontrolled process costs. Thus, an HDS process operated at mild temperature and pressure over a low-cost catalyst without compromising on the process efficiency could offer an alternative route for fuel oil processing.

Apart from HDS, a newer approach to fuel oil desulfurization research is extraction using ionic liquids (ILs).[14,15] Aspects such as ease of synthesis, high recycling ability, low volatility, high thermal stability and environmental friendliness are credited for the widespread application of ILs.[16] However, few studies on the integrated application of ILs with solid catalysts have been reported in hydrogenation reactions,[17] which emphasizes that ILs coupled with solid catalysts should be tested for HDS of fuel oils.

In previous work, we reported 52% dibenzothiophene (DBT) conversion in a HDS process with a mild operating temperature and pressure by the coupled application of selected ILs with Ce–Ni–Mo/Al_2O_3 catalysts.[18] However, to further improve the efficiency of solid catalyst-coupled ILs HDS processes, more exploration is required for new types of catalysts and ILs.

[a]*School of Chemistry and Chemical Engineering, Key Laboratory of Petrochemical Resource Processing and Process Intensification Technology, Guangxi University, Guangxi, 530004, P. R. China. E-mail: zhftong@sina.com*

[b]*Institute of Chemical Sciences, University of Peshawar, Peshawar, 25120, KP, Pakistan*

[c]*Department of Chemistry, Umea University, Umea, Sweden*

† Electronic supplementary information (ESI) available. See DOI: 10.1039/c9ra00095j

Pd has been reported as a more promising promoter for classical HDS catalysts than many of its counterparts, *e.g.* Ir and Ru.[19,20] However, to our knowledge, no studies on the HDS of DBT coupled with ILs using Pd-promoted Co–Mo/Al_2O_3 and Ni–Mo/Al_2O_3 catalysts at mild operating conditions have been reported so far. Extractive desulfurization by ILs can augment the hydrogenation by solid catalysts in their blended application at mild operating conditions. Low Pd loading and mild operating conditions can concomitantly lead to cost-effectiveness and process safety. Thus, in this work, HDS of DBT was performed at 120 °C temperature and 1 MPa H_2 pressure over low (0.5 wt%) Pd-loaded Co–Mo/Al_2O_3 and Ni–Mo/Al_2O_3 sulfide phase catalysts coupled with selected ILs. The fresh and spent catalysts were characterized by X-ray photoelectron spectroscopy (XPS), field emission scanning electron microscopy (FESEM), inductively coupled plasma mass spectrometry (ICP-MS), energy dispersive X-ray (EDX), X-ray diffraction (XRD) and BET surface area techniques. The reaction products were quantitatively and qualitatively analyzed *via* high-pressure liquid chromatography (HPLC) and gas chromatography coupled with mass spectrometry (GC-MS), respectively, and a suitable reaction mechanism was proposed.

2. Materials and methods

2.1. Chemicals

All the reagents used in this study were of analytical reagent grade and were used without further purification. DBT, *n*-octane, the Al_2O_3 support and $Ni(NO_3)_2 \cdot 4H_2O$ were purchased from Sinopharm Chemical Reagent Co. Ltd. $Co(NO_3)_2 \cdot 6H_2O$

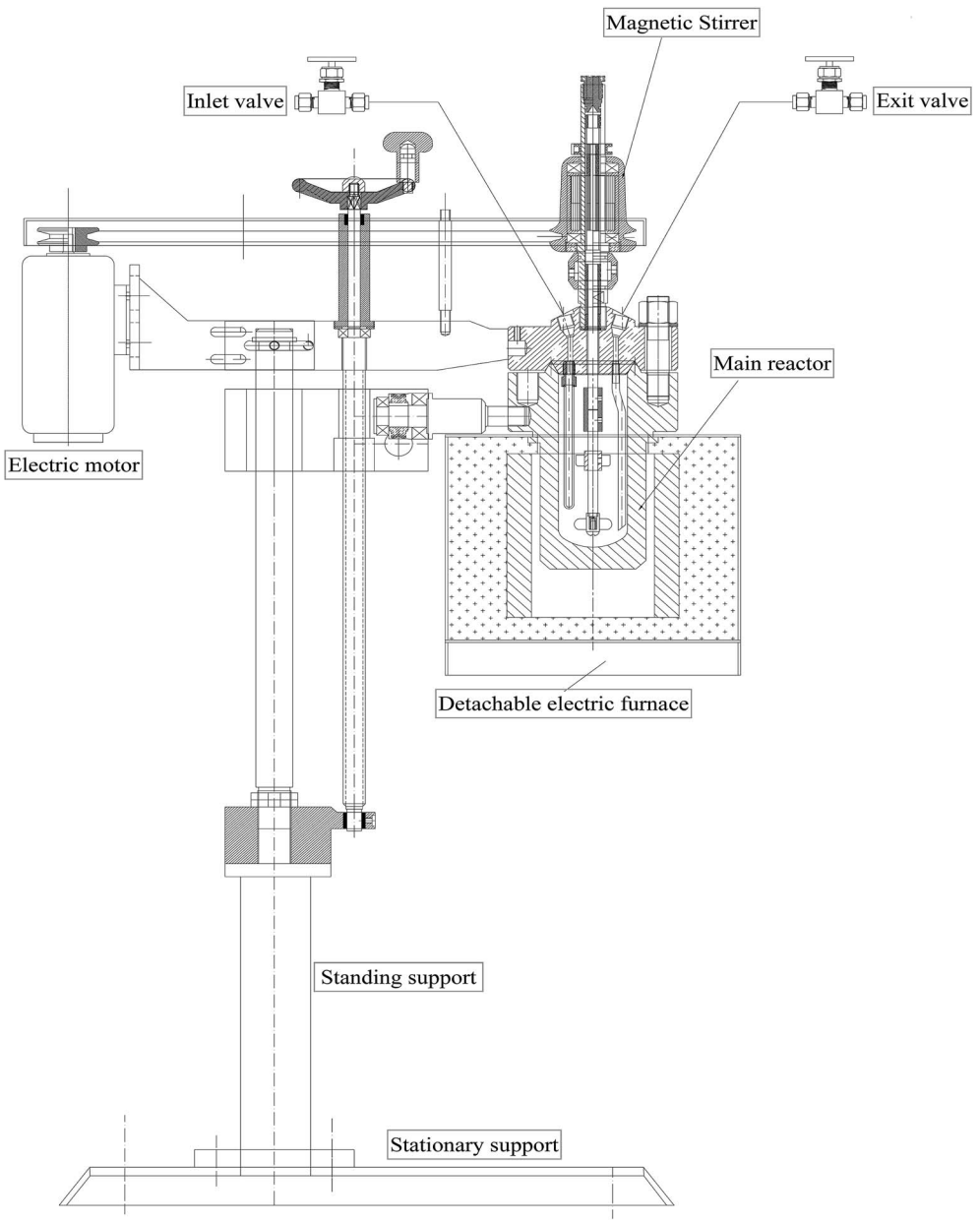

Fig. 1 Design of the batch autoclave reactor.

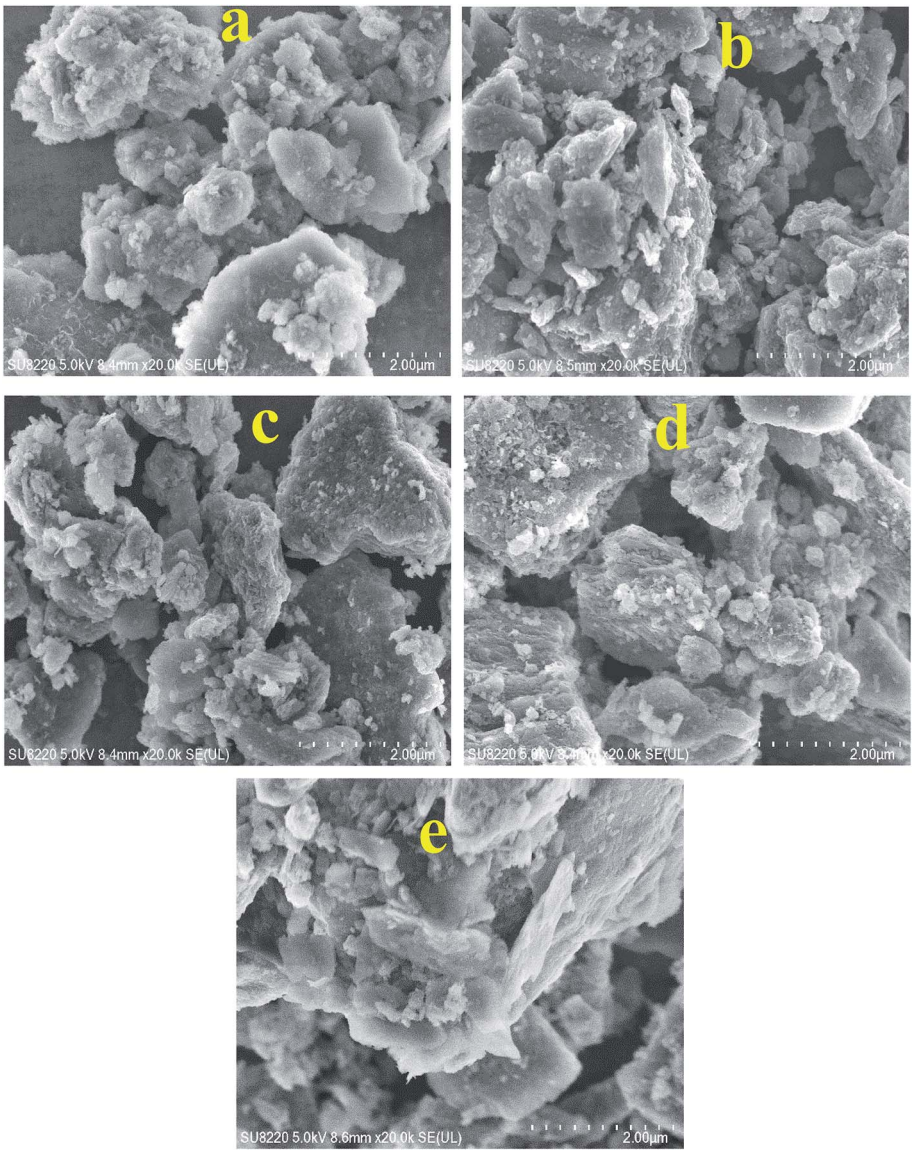

Fig. 2 FESEM images of (a) Al_2O_3 and the fresh catalysts (b) Co-M/Al_2O_3, (c) Ni–Mo/Al_2O_3, (d) Pd–Co–Mo/Al_2O_3 and (e) Pd–Ni–Mo/Al_2O_3.

was obtained from Tian Jin Shifu Chen Chemical Reagent Factory, China. Ammonium heptamolybdate ($(NH_4)_6Mo_7O_{24}\cdot 4H_2O$) was purchased from Jin Mao Chemical Reagent Co. Ltd, while palladium chloride ($PdCl_2$) was provided by Sa En Chemical Technology, Co. Ltd. Shang Hai, China. Five different ILs were purchased from Shanghai Cheng Jie Chemical Co. Ltd. China. Pure H_2 gas was used in all hydrogenation experiments.

Table 1 Surface porosity data for fresh and spent catalysts used in HDS under 1 MPa H_2 pressure, 4 h reaction time and 120 °C temperature coupled with $[(C_8H_{17})(C_4H_9)_3P]Br$

Sample	BET surface area ($m^2\ g^{-1}$)		Langmuir surface area ($m^2\ g^{-1}$)		Pore volume ($cm^3\ g^{-1}$)		Pore diameter (nm)	
	Fresh	Spent	Fresh	Spent	Fresh	Spent	Fresh	Spent
Al_2O_3	200.8	—	291.5	—	0.30	—	6.0	—
Co–Mo/Al_2O_3	109.6	99.1	156.6	148.5	0.21	0.19	7.7	7.6
Ni–Mo/Al_2O_3	120.5	91.9	172.5	138.0	0.22	0.17	7.4	7.5
Pd–Co–Mo/Al_2O_3	115.1	72.5	164.2	109.4	0.22	0.16	8.0	9.0
Pd–Ni–Mo/Al_2O_3	108.4	79.9	155.0	119.8	0.22	0.17	8.2	8.6

2.2. Experimental

2.2.1. Catalyst preparation. Four types of catalysts were prepared using the incipient impregnation method reported elsewhere.[2] A known amount of Al_2O_3 support was sequentially impregnated *via* stirring with a known amount of precursor salt solution of Co, Ni, Mo, or Pd, each corresponding to 2, 4, 8, and 0.5 wt%, respectively, at 200 rpm and room temperature for 24 h. The solutions were then dried in an oven at 110 °C for 12 h and subsequently calcined in a muffle furnace at 500 °C for 5 h. The calcined catalysts were then presulfided in a tubular furnace at 500 °C for 6 h using 20% CS_2 solution in cyclohexane in a N_2 flow at a rate of 100 mL min^{-1} and 2 MPa pressure. The presulfided catalysts were stored under N_2 atmosphere.

2.2.2. Catalyst characterization. Fresh and spent catalysts were characterized for surface morphology, elemental composition and distribution *via* field emission scanning electron microscopy (FESEM SU-8220N, Hitachi, Japan), ICP-MS (PerkinElmer NexION™ 350D) and EDX techniques. BET surface area measurements were performed *via* N_2 adsorption method using a Micromeritics Gemini VII surface area and porosity analyzer. Crystal structure and phase characterizations were achieved *via* XRD (Rigaku Smartlab, X-ray diffractometer, Japan) operated at 9 kW with a scan speed of 10° min^{-1} in the 2θ angular range of 5–80°. The surface elemental composition and electronic states of various metals in the catalysts were characterized by XPS (Thermo Electron Corporation, USA).

2.2.3. Measurement of HDS catalytic activity. Catalytic activity tests were performed in a 200 mL stainless steel batch autoclave reactor heated by an electrical furnace (Fig. 1) and connected to a temperature and stirrer console. In a typical experiment, the reactor was charged with 30 mL of 1000 ppm DBT solution in *n*-octane, 0.1 g of presulfided catalyst and a fixed mass of IL. After sealing, the reactor was evacuated of air *via* a vacuum pump for 15 min three times with purges of H_2 at every step at a pressure of 3 MPa. Finally, the reactor was charged with H_2 gas to the desired pressure and then heated to a known temperature at a heating rate of 5 °C min^{-1}. The different reaction parameters, *i.e.* type of catalyst, type of IL, H_2

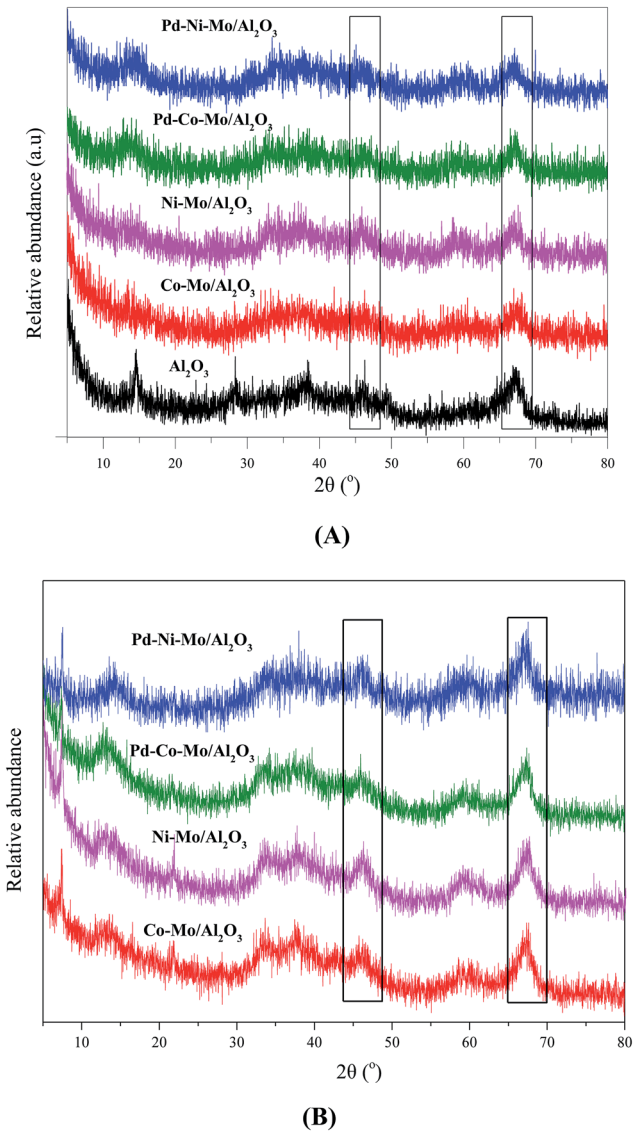

Fig. 3 XRD patterns of (A) support and fresh catalysts and (B) spent catalysts.

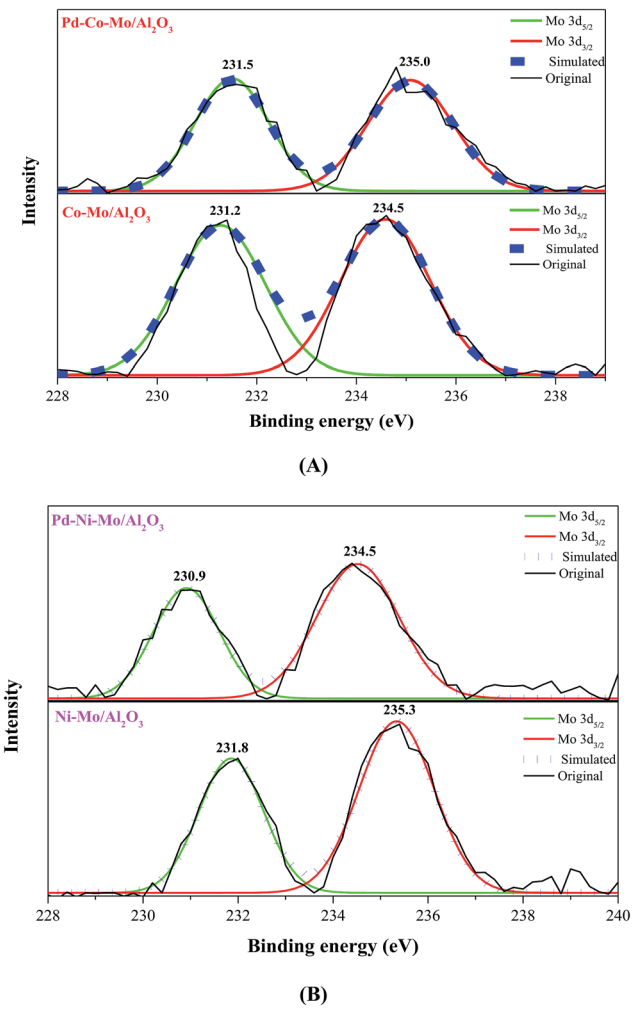

Fig. 4 High-resolution XPS spectra of Mo 3d (A) Co–Mo/Al_2O_3 and Pd–Co–Mo/Al_2O_3 and (B) Ni–Mo/Al_2O_3 and Pd–Ni–Mo/Al_2O_3 catalysts.

pressure, temperature, and oil : IL ratio, were separately optimized.

The catalytic activity in terms of DBT conversion (%) was calculated using eqn (1):

$$\text{DBT conversion (\%)} = \left[\frac{C_o - C_i}{C_o}\right] \times 100 \quad (1)$$

where C_o and C_i are the DBT concentrations before and after the reaction, respectively.

2.2.4. Product analysis. HDS products were quantitatively analyzed *via* HPLC (Agilent 1100 using a Zorbax SB-C18 column with dimensions of 4.6 × 150 mm) with a UV detector at a wavelength of 320 nm^2 applying the calibration curve shown in Fig. S1.† Qualitative analyses were performed on a GC-MS chromatograph (Agilent 7890A with a DB-5MS stainless steel column 30 m in length with an inner diameter of 0.25 mm) coupled with a mass spectrometer (MS-5975C). Each GC-MS run utilized 2 μL of sample and was heated from room temperature to 80 °C in one minute, then increased to 250 °C at a heating rate of 10 °C min^{-1} till the end of the run.

3. Results and discussion

3.1. Characterization of catalysts

Fig. 2 shows the FESEM images of pure Al_2O_3 and fresh Co–Mo/Al_2O_3, Ni–Mo/Al_2O_3, Pd–Co–Mo/Al_2O_3, and Pd–Ni–Mo/Al_2O_3 catalysts while Fig. S2† summarizes the FESEM images of spent versions of these catalysts. The data in Table 1 and FESEM images in Fig. 2a reveal the highly porous nature of the Al_2O_3 support. Fig. 2b shows that uniformly deposited Mo and Co species led to a decrease in the porosity and surface area and an increase in the particle size compared to those of the pure support (Table 1).[21–23] The bimetallic Co–Mo/Al_2O_3 and Ni–Mo/Al_2O_3 catalysts possessed less compact morphology (Fig. 2(b and c)) than those of trimetallic Pd–Co–Mo/Al_2O_3 and Pd–Ni–Mo/Al_2O_3 (Fig. 2(d and e)). The spent catalysts (Fig. S2(a–d)†) (tested in HDS reaction at optimized conditions of 4 h, 1 MPa H_2 pressure at 120 °C using an oil : IL ratio of 10 : 3.3) suffered a significant decrease in porosity, resulting in the appearance of clots with an overall increase in particle size and pore diameter (Table 1).[24] This could be due to the deposition of DBT or HDS products, and preferential utilization of micro- and meso-pores during the HDS reaction.[25] Compared to the spent Co–Mo/Al_2O_3 and Ni–Mo/Al_2O_3 catalysts in Fig. S2(a and b),† the spent Pd-promoted (Pd–Co–Mo/Al_2O_3 and Pd–Ni–Mo/Al_2O_3) catalysts in Fig. S2(c and d)† exhibited a much more compact and packed morphology, which might be the result of more sulfur species deposited being deposited owing to their much higher DBT conversion than Co–Mo/Al_2O_3 and Ni–Mo/Al_2O_3 (to be discussed in the following sections).

The ICP-MS results in Table S1† advocate lower concentrations of the impregnated metals in the four types of catalysts than the theoretical values, which could be attributed to the leaching of some metal species during the catalyst synthesis or improper dissolution of the catalysts for ICP analysis, especially for the Pd-based catalysts. The concentration of all metals in the spent catalysts was considerably decreased, which could be attributed to their agglomeration (FESEM images in Fig. S2†) or disposition of HDS products after being tested in the HDS of DBT. The EDX spectrum (Fig. S3(a)†) of the Al_2O_3 support shows abundant Al and O species. Fig. S3(b–e)† confirms the successful impregnation of Co, Ni, Mo and Pd onto the Al_2O_3 support.[26] Furthermore, the EDX elemental mappings for the fresh catalysts in Fig. S4A† suggest the uniform distribution of Co, Ni, Mo and Pd over the support surface, which was considerably decreased for the spent catalysts (Fig. S4B†), which

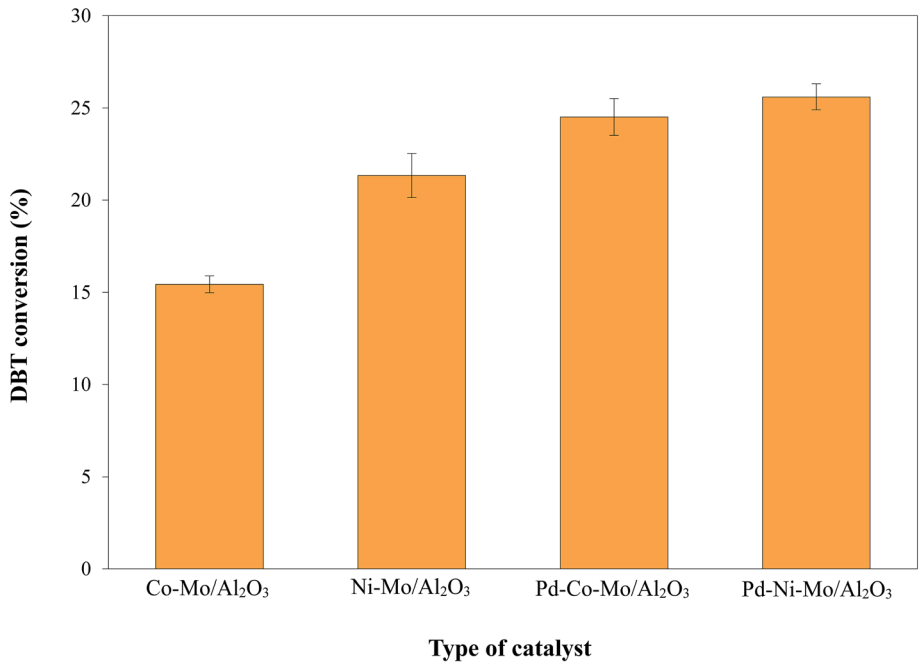

Fig. 5 DBT conversion by 0.1 g of presulfided catalyst at 3 MPa H_2 pressure, 160 °C and 4 h reaction time using 30 mL of 1000 ppm DBT solution.

was attributed to the blockage of the surface by DBT molecules in the latter. Moreover, the EDX elemental mapping results further confirmed that Mo had the densest distribution ((Fig. S4A(g–j) and S4B(r–u)†) while Pd had the lowest distribution density (Fig. S4A(e and f) and S4B(p and q)†). Al present in the bulk in the Al_2O_3 support possessed the densest distribution (Fig. S4A(k)†).

Porosity, specific surface area (SSA) and Langmuir surface area data for the Al_2O_3 support and various catalysts are provided in Table 1. The SSA of the support was considerably decreased upon the impregnation of Co, Ni, Mo and Pd.[7,27] The hysteresis loop at higher relative pressure ($P/P_o > 0.6$) in Fig. S5† indicates the predominant presence of micropores and mesopores.[28] Spent catalysts (tested in HDS reaction for 4 h, 1 MPa H_2 pressure at 120 °C using an oil : IL ratio of 10 : 3.3) exhibited a significantly high decrease in SSA, which could be attributed to the deposition of DBT or HDS products.[29] The decrease in the SSA and increase in the pore diameter after the addition of Co or Ni to the Al_2O_3 support and Pd to the Co–Mo/Al_2O_3 or Ni–Mo/Al_2O_3 catalysts could be attributed to the increase in mesoporosity.[30] In the case of the spent catalysts (Table 1), the net increase in the pore diameter and decrease in the pore volume could be owing to the preferential utilization of micro- and meso-pores during the HDS reaction, leaving macropores behind with their larger pore diameter.[30]

The XRD patterns of Al_2O_3 and fresh catalysts compiled in Fig. 3 suggest a high degree of dispersion with a minimum degree of crystallization. Fig. 3A shows strong peaks for Al_2O_3 at 2θ of 47° and 67° (black rectangles),[31,32] which were weakened by the incorporation of Co, Ni, Mo or Pd, suggesting that the catalysts maintained the proper pore structure required for the HDS reaction. The peaks at 2θ of 33° and 59° were ascribed to MoS_2 species in all catalysts[33,34] while Ni showed a weak peak at 2θ of 60° in Ni–Mo/Al_2O_3 and Pd–Ni–Mo/Al_2O_3.[35] The XRD patterns of the spent catalysts shown in Fig. 3B indicate that there was little change in the bulk structure compared with those of the fresh catalysts (Fig. 3A) suggesting their stable nature under the current HDS reaction conditions.[36] However, from the XRD patterns in Fig. 3B, one can see the decrease in the dispersion of metallic species as the peaks become sharper compared to the fresh catalysts (Fig. 3A), which could be due to the deposition of sulfur moieties after the HDS reaction. It can be concluded from Fig. 3(A and B) that with low metal loading, specifically of Pd, and a highly amorphous nature with a high degree of dispersion of the catalyst (Fig. S4A and S4B†), the XRD data provided little information about the exact composition and crystallinity of the individual species[18,33]. Furthermore, the low metal loading of Pd (0.5 wt%) was below the detection limit of the XRD instrument and hence no clear peak appeared for Pd in the Pd–Co–Mo/Al_2O_3 or Pd–Ni–Mo/Al_2O_3 catalysts.

The full survey XPS spectra of the four types of fresh catalysts are shown in Fig. S6(I),† confirming the presence of Co, Mo, Ni and Al. In Fig. S6(I),† the presence of a large amount of C 1s could be owing to the presence of organic compounds or the C left from cyclohexane in the presulfidation step.[37] The Co–Mo/Al_2O_3 catalyst in Fig. 4A exhibited two prominent peaks at

Table 2 Molecular and structural formulae of ILs tested in catalytic HDS of DBT

Molecular formula	Structural formula
[EMIM]BF_4	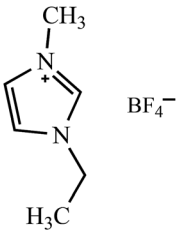
[BMIM]BF_4	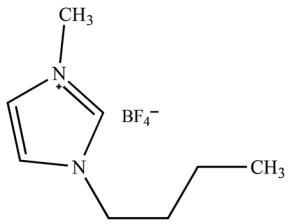
[EMIM]$AlCl_4$	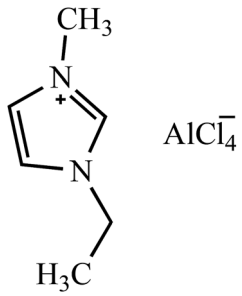
$[(CH_3)_4N]Cl$	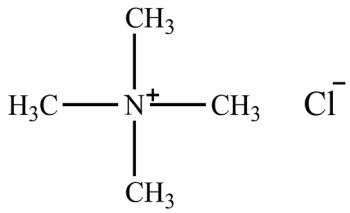
$[(n\text{-}C_8H_{17})(C_4H_9)_3P]Br$	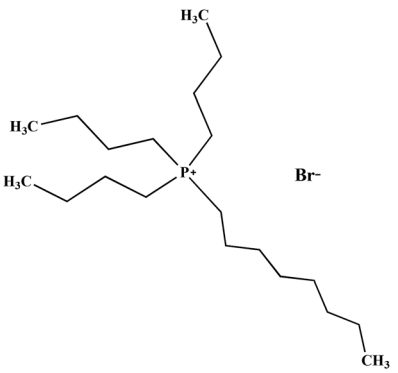

binding energies (BE) of 231.2 eV and 234.5 eV ascribed to Mo $3d_{5/2}$ and Mo $3d_{3/2}$ as MoS_3 phase, respectively.[38,39] Elemental Mo (at 227.5 or 230.6 eV)[39] was not detected in any of the samples, indicating the complete sulfidation of Mo species. The shift towards higher BE of Mo $3d_{5/2}$ (231.5 eV) and Mo $3d_{3/2}$ (235.0 eV) (Fig. 4A) for Pd–Co–Mo/Al_2O_3 compared to those in Co–Mo/Al_2O_3 could be attributed to the stronger interaction of

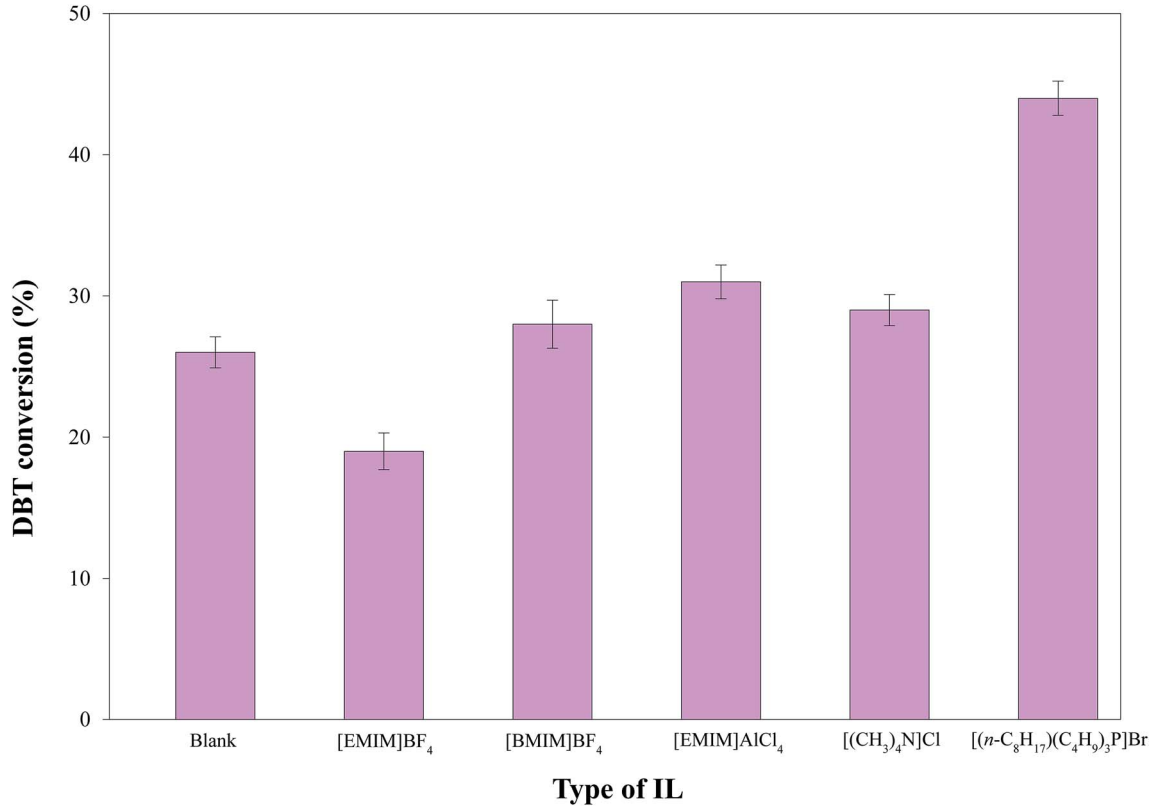

Fig. 6 Comparison of DBT conversion by Pd–Ni–Mo/Al_2O_3 (0.1 g) combined with 4 g of each IL at 160 °C, 3 MPa H_2 pressure, and 4 h reaction time with 30 mL of 1000 ppm DBT solution.

Mo with Pd in the former. On the contrary, the lower BE for Mo $3d_{5/2}$ and $3d_{3/2}$ (230.9 and 234.5, respectively) in Pd–Ni–Mo/Al_2O_3 than those for the same two states in Ni–Mo/Al_2O_3 (231.8 and 235.3, respectively) in (Fig. 4B) was indicative of a weaker interaction between Mo and Pd species in Pd–Ni–Mo/Al_2O_3, leading to better dispersion of the active phase, which can play an active role in enhancing the catalytic activity towards DBT conversion. The degree of interaction of Pd with Mo in the Pd–Co–Mo/Al_2O_3 and Pd–Ni–Mo/Al_2O_3 catalysts could be justified by a charge compensation model in which Mo loses d-electrons and gains sp-electrons while Pd gains d-electrons and loses sp electrons.[40] The weaker interaction of Pd with Ni in the Pd–Ni–Mo/Al_2O_3 catalyst (lower BE in Fig. 4B) could be attributed to stronger Ni–Mo interaction owing to the $3d^8 4S^0$ configuration than that in the Pd–Co–Mo/Al_2O_3 catalyst (with $3d^7 4S^0$ configuration).[41] In brief, XPS analysis indirectly confirmed the extremely low loading of Pd (0.5 wt%) in Pd–Co–Mo/Al_2O_3 and Pd–Ni–Mo/Al_2O_3 catalysts, which was not achieved by XRD analysis. A similar trend can be observed in Fig. S6(II and III)† showcasing the S $2p_{3/2}$ and S $2p_{1/2}$ states in various catalysts.[41]

3.2. Catalytic HDS activity tests

HDS catalytic activity tests of the presulfided catalysts were performed in a 200 mL batch autoclave reactor (Fig. 1) as detailed in Section 2.2.3. Different reaction parameters were independently optimized, as discussed below.

3.2.1. HDS activity of different catalysts and effect of Pd incorporation. Four types of sulfide phase catalysts *i.e.* Co-M/Al_2O_3, Ni–Mo/Al_2O_3, Pd–Co–Mo/Al_2O_3 and Pd–Ni–Mo/Al_2O_3 (each 0.1 g) were separately tested for HDS activity in the absence of IL at 160 °C, 4 h reaction time, 3 MPa H_2 pressure, and 200 rpm stirring speed utilizing 30 mL of a 1000 ppm DBT model solution. The results in Fig. 5 indicate that the Ni-based catalysts exhibited higher catalytic activity than the Co-based catalysts, which is attributed to the higher reduction potential of Ni with $3d^8 4S^0$ configuration (higher affinity towards the electron-rich sulfur center in DBT) than that of Co with $3d^7 4S^{02}$ configuration. Furthermore, the lower adsorption strength over the Al_2O_3 support of Ni compared to Co allows the Ni to remain on the surface without forming aluminate ions[42] and ultimately facilitates higher chances of DBT hydrogenation. The enhanced activity of the Pd-promoted catalysts was obviously due to the extra Pd active phase,[43] better dispersion of Co, Ni and Mo species by the incorporation of Pd, and hindrance of sintering and clotting.[44] From Fig. 5, the HDS activity order of the various catalysts was found to be: Pd–Ni–Mo/Al_2O_3 > Pd–Co–Mo/Al_2O_3 > Ni–Mo/Al_2O_3 > Co–Mo/Al_2O_3.

3.2.2. Process and mechanism of HDS by the solid catalyst-IL coupled system. The selected ILs (4 g; Table 2) coupled with 0.1 g of Pd–Ni–Mo/Al_2O_3 catalyst in the HDS of 30 mL of 1000 ppm DBT solution at 160 °C temperature, 3 MPa H_2 pressure, 200 rpm stirring speed and 4 h reaction time were separately tested. The results in Fig. 6 indicate that [BMIM]BF_4,

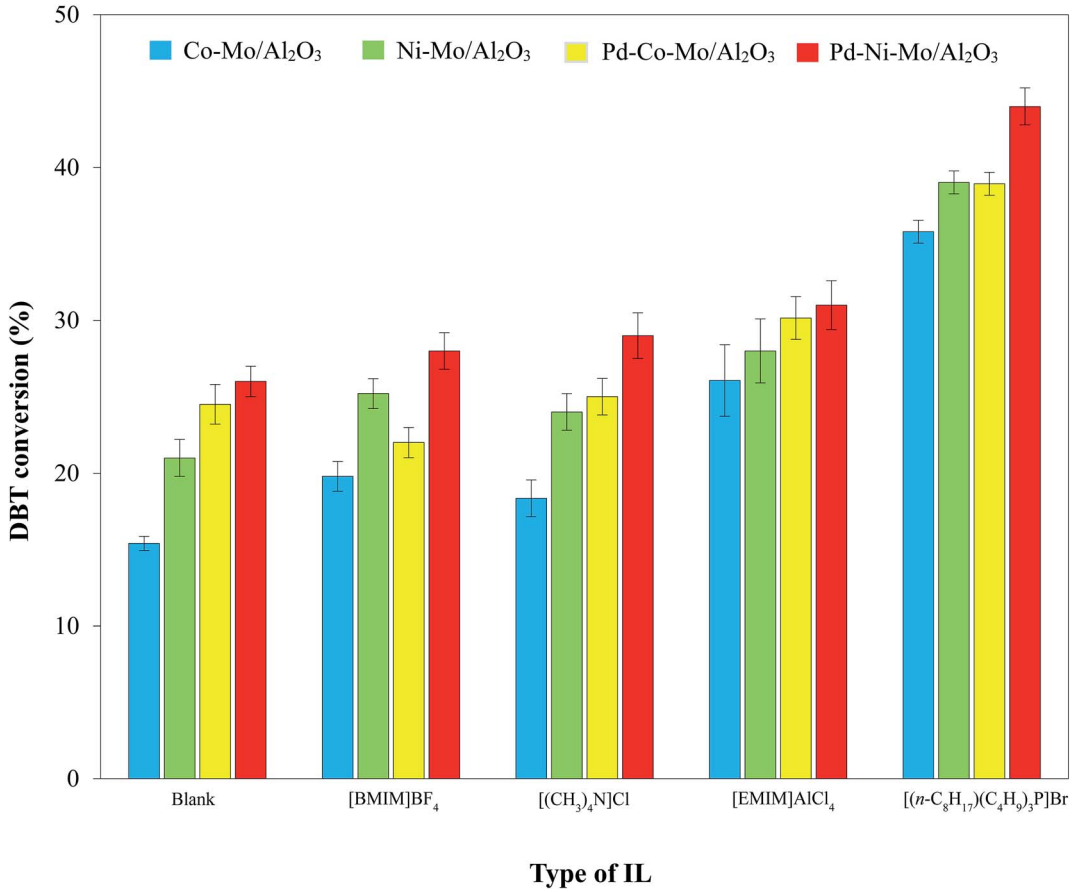

Fig. 7 Comparison of DBT conversion by different catalysts (0.1 g) combined with 4 g of each IL at 160 °C, 3 MPa H_2 pressure and 4 h reaction time using 30 mL of 1000 ppm DBT solution.

$[EMIM]AlCl_4$, $[(CH_3)_4N]Cl$, and $[(n\text{-}C_8H_{17})(C_4H_9)_3P]Br$ coupled with the solid catalyst exhibited higher HDS activity than blank catalysts, which could be attributed to certain electronic factors. The nature and structure of the anions and cations of ILs play crucial roles in their desulfurization efficiency.[45] For example, in $[BMIM]BF_4$ and $[EMIM]BF_4$, the higher desulfurization efficiency of the former could be attributed to the longer cation chain.[45] The higher HDS of DBT by the coupled application of ILs with the solid catalyst was owing to the synergistic effect of extraction by the ILs[18,46–48] and hydrogenation by the solid catalyst. The extraction of DBT by IL is owing to the insertion of sulfur from DBT (with conjugation between the lone pair on S and the π electrons of the aromatic ring) into the dynamic structure of the IL.[49] $[EMIM]AlCl_4$ produces $AlCl_4^-$ and $Al_2Cl_7^-$ ions in the solution phase, which drastically enhances its extractive efficiency towards DBT.[46] Similarly, $[(CH_3)_4N]Cl$ possesses outstanding extraction ability[45] and hence led to enhanced DBT conversion coupled with the solid catalyst. The highest DBT conversion by $[(n\text{-}C_8H_{17})(C_4H_9)_3P]Br$ coupled with Pd–Ni–Mo/Al_2O_3 in Fig. 6 and 7 was accredited to its superior extraction ability, higher thermal stability, higher solubility of polarizable delocalized bonds of DBT and van der Waals forces than the other tested ILs.[50] Similarly, the higher conversion by quaternary cation-based ILs, *i.e.* $[(CH_3)_4N]Cl$ and $[(n\text{-}C_8H_{17})(C_4H_9)_3P]Br$, could also be attributed to their cation–anion interaction being looser than those of the other ILs, while the longer cation chain of $[(n\text{-}C_8H_{17})(C_4H_9)_3P]Br$ compared to $[(CH_3)_4N]Cl$ resulted in higher desulfurization efficiency of the former.[45] In addition, the higher DBT conversion by $[(n\text{-}C_8H_{17})(C_4H_9)_3P]Br$ could also be owing to the looser bond between phosphonium and its anion than that of ammonium with the corresponding anion and the higher thermal stability of the former than the latter. Under identical experimental conditions, the other three types of catalyst, *i.e.*, Co–Mo/Al_2O_3, Ni–Mo/Al_2O_3 and Pd–Co–Mo/Al_2O_3, followed a similar activity trend (Fig. 7) to that in Fig. 6. $[(n\text{-}C_8H_{17})(C_4H_9)_3P]Br$ was selected for subsequent experiments owing to its maximum DBT conversion efficiency coupled with the solid catalyst.

Table 3 Catalytic/extractive performance in terms of DBT conversion by 4 g of $[(n\text{-}C_8H_{17})(C_4H_9)_3P]Br$ coupled with HDS reaction (in the absence of a solid catalyst) at 160 °C, 4 h reaction time, 200 rpm and 3 MPa H_2 pressure

Type of experiment	Type of IL	H_2 pressure (MPa)	DBT conversion (%)
Extraction	$[(n\text{-}C_8H_{17})(C_4H_9)_3P]Br$	—	13
Extraction with HDS	$[(n\text{-}C_8H_{17})(C_4H_9)_3P]Br$	3	22

The catalytic role of ILs coupled with solid catalysts was further analyzed by performing experiments in the same autoclave reactor without the addition of Pd–Ni–Mo/Al_2O_3 over 4 g of [(n-C_8H_{17})(C_4H_9)$_3$P]Br IL with 200 rpm stirring speed and 160 °C temperature for 4 h using 30 mL of 1000 ppm DBT solution. After the reaction, the concentration of DBT in the oil phase (separated by decantation) was analyzed by HPLC. The results in Table 3 suggest that DBT extraction by mere [(n-C_8H_{17})(C_4H_9)$_3$P]Br (13%) was enhanced by combining it with HDS (22%). From these results, one can conclude that [(n-C_8H_{17})(C_4H_9)$_3$P]Br along with extraction also played a catalytic role to a certain extent in combination with HDS. This synergistic effect was further enhanced by the introduction of the Pd–Ni–Mo/Al_2O_3 catalyst to the reaction medium (Fig. 6 and 7), enhancing the DBT conversion from 26% to 44% (Fig. 6).

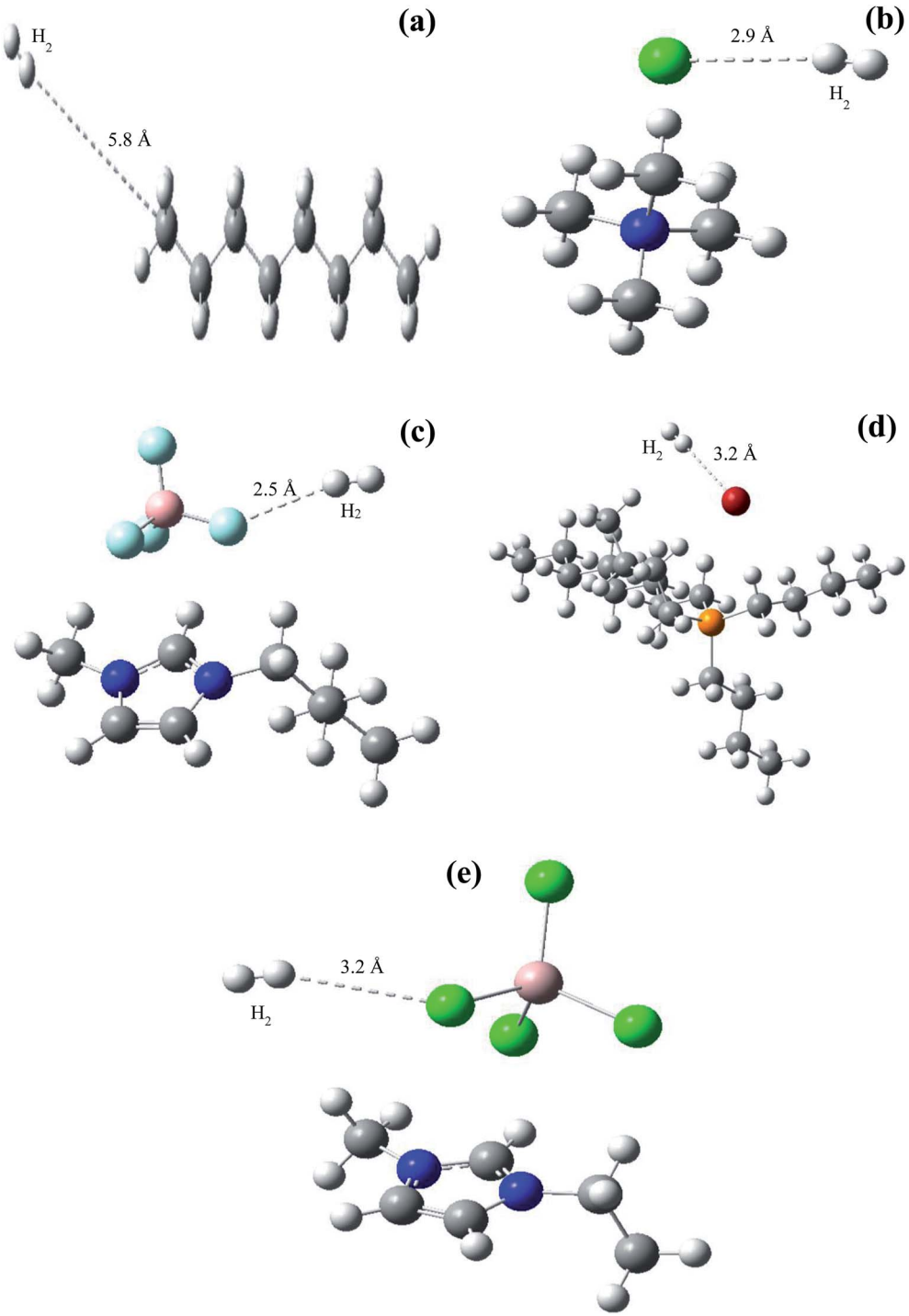

Fig. 8 DFT simulation indicating interaction of H_2 with (a) n-octane, (b) [$(CH_3)_4$N]Cl, (c) [BMIM]BF_4, (d) [(n-C_8H_{17})(C_4H_9)$_3$P]Br and (e) [EMIM]$AlCl_4$ in terms of binding energy and relative distance between atoms.

Table 4 DFT simulation data in terms of binding energy of H_2 interaction with *n*-octane and different types of IL

Sample	Binding energy (uncorrected) kJ mol^{-1}	BSSE correction factor	Binding energy (corrected) kJ mol^{-1}
n-Octane	0.029	0.004	0.033
$[(CH_3)_4N]Cl$	−3.77	0.321	−3.449
$[BMIM]BF_4$	−2.64	0.378	−2.262
$[(n\text{-}C_8H_{17})(C_4H_9)_3P]Br$	−2.75	0.091	−2.659
$[EMIM]AlCl_4$	−1.19	0.366	−0.824

The effect of the ILs-solid catalyst coupled system on HDS was further validated *via* DFT simulation using Gaussian 3 software (Fig. 8) and the resulting BE are provided in Table 4. The geometries of the reacting species were optimized at the B3LYP/6-311+g(d,p) level, both with and without BSSE corrections, while the geometry parameters of each IL with H_2 are shown in Table S2.† The relative distance between H_2 and the terminal C atom of *n*-octane (Fig. 8a) was much larger (5.8 Å) than that between H_2 and the anionic center of the ILs (Fig. 8b–e and Table 4), suggesting a stronger interaction between the latter pair. Furthermore, the BE between H_2 and ILs in Table 4 were much smaller than those between H_2 and *n*-octane, confirming the higher solubility of H_2 in IL than in *n*-octane. This can facilitate easier mass transfer of H_2 through the IL and hence better chances of activated H atom generation[51] which can, in turn, enhance the HDS activity. Better H_2 solubility in ILs is envisaged in Fig. 9. A heterogeneous catalytic process, *e.g.*, HDS, is controlled by the adsorption of H_2 gas onto the surface of the solid catalyst. As illustrated in Fig. 9, H_2 gas introduced into the reactor faces and penetrates through the barrier of the oil phase (DBT solution) followed by the film between the oil phase and the solid catalyst and finally reaches and spreads

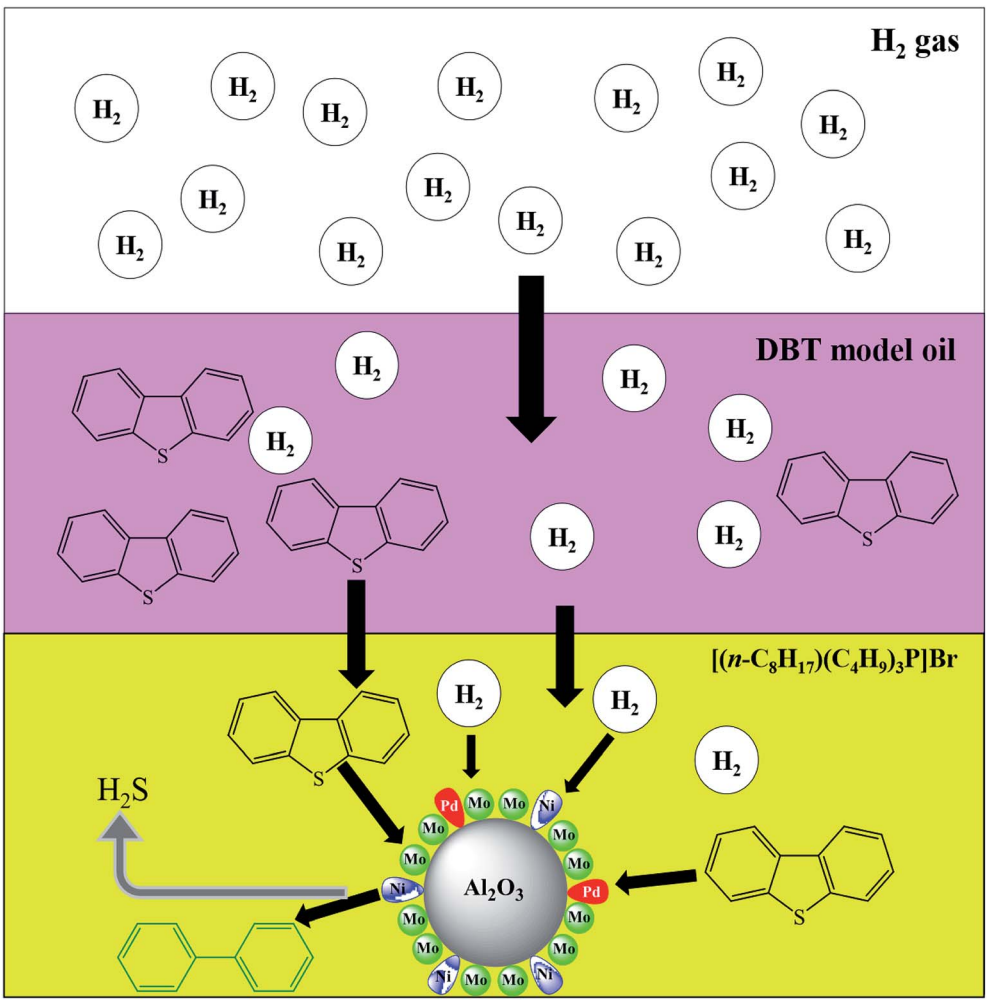

Fig. 9 HDS of DBT process demonstrating transport of H_2 through oil and IL phase reaching the solid catalyst surface.

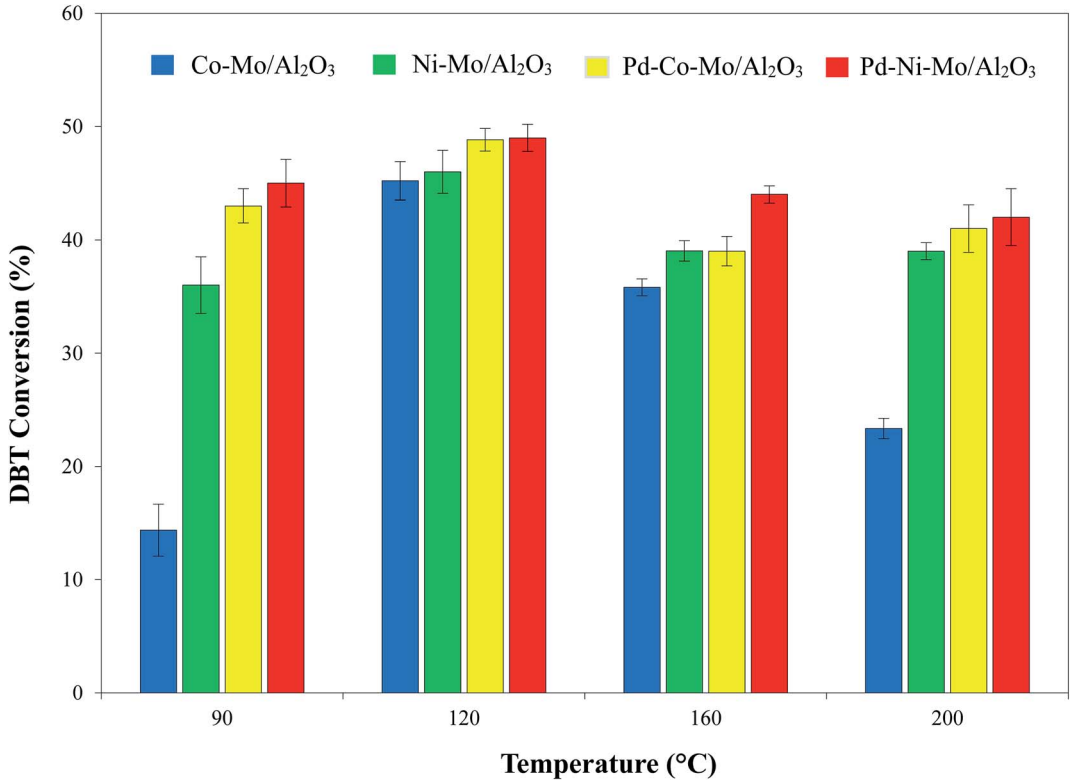

Fig. 10 Effect of reaction temperature on DBT conversion utilizing 0.1 g of each catalyst at 3 MPa H_2 pressure, 4 h reaction time, 200 rpm stirring speed, 30 mL of 1000 ppm DBT solution and 4 g of [(*n*-C_8H_{17})(C_4H_9)$_3$P]Br.

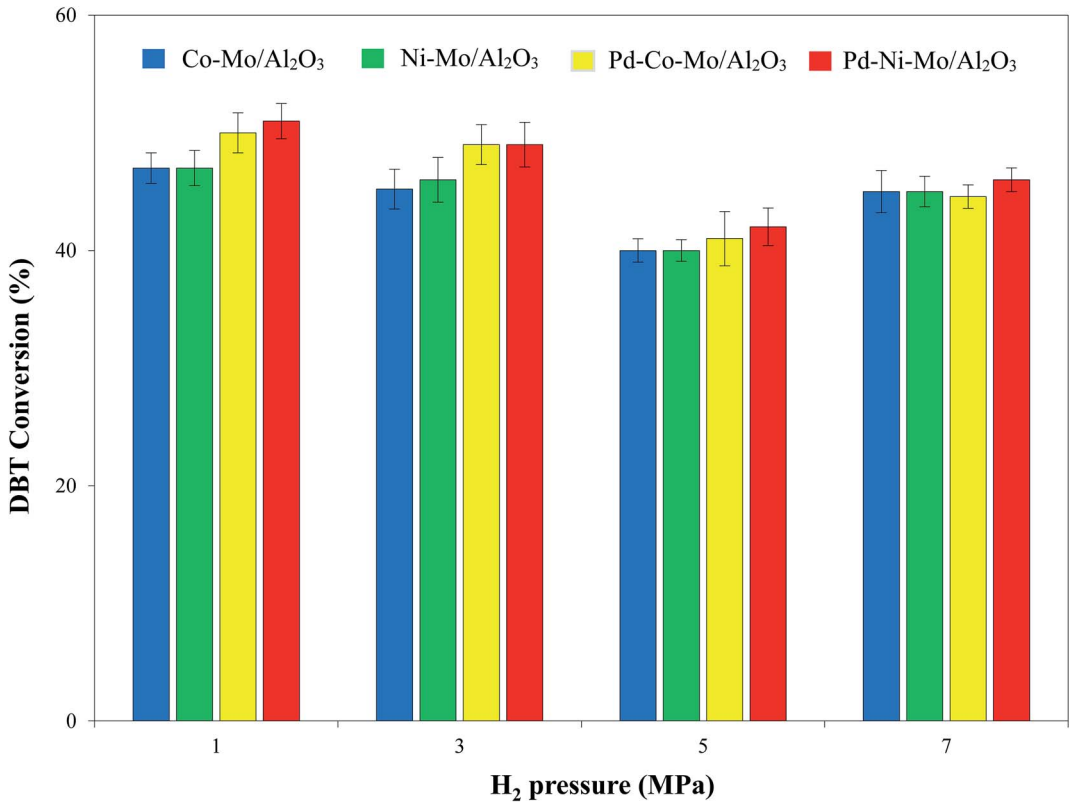

Fig. 11 Effect of H_2 pressure on the HDS activity of different catalysts (0.1 g each) in the presence of 4 g of [(*n*-C_8H_{17})(C_4H_9)$_3$P]Br at 120 °C and 4 h reaction time and 30 mL of 1000 ppm DBT solution.

over the surface of the Pd–Ni–Mo/Al_2O_3 catalyst. Over the catalyst surface, H_2 is activated into H atoms and then performs the HDS reaction of DBT. In this scenario, the solubility of H_2 in the liquid phase is the major activity-controlling factor.[51] The DFT results in Fig. 8 show the much higher solubility of H_2 in all of the four ILs than in the DBT model oil, which is conducive to better H_2 transport through the reaction mixture in the presence of IL, allowing the H_2 to reach and then be activated on the surface of the Pd–Ni–Mo/Al_2O_3, ultimately performing the HDS reaction. Thus, one can conclude that ILs concomitantly act as DBT extractants as well as enhancing the solubility of H_2, which augmented the HDS activity of the solid catalyst and hence recorded better activity than that of the blank catalysts.

3.2.3. Effect of reaction temperature on the HDS activity. The effect of mild reaction temperatures (90–200 °C) on the catalytic HDS of DBT coupled with [(*n*-C_8H_{17})(C_4H_9)$_3$P]Br IL (4 g) shown in Fig. 10 indicates the higher activity of the IL-coupled system than of the blank catalysts owing to the synergistic effect of the catalytic desulfurization reaction (by H_2) and extraction (by IL).[18] Increasing the temperature from 90 to 120 °C leads to a decrease in the viscosity of the IL, facilitating better H_2 solubility,[52] and can also provide the activation energy for the reaction, thus leading to a corresponding increase in DBT conversion. However, temperatures beyond 120 °C may lead to reverse migration of DBT to the solution media according to Van't Hoff law, hence decreasing the DBT conversion.[50] Apart from this, increasing the temperature beyond 120 °C may lead to the dissociation of the IL,[18] hence diminishing the synergistic effect of the IL coupled with the solid catalyst, and a decrease in DBT conversion is observed. Another reason could be the decreased solubility of H_2 in the IL or *n*-octane beyond 120 °C.[53] At the optimized 120 °C, a maximum DBT conversion of 50% was recorded for Pd–Ni–Mo/Al_2O_3 coupled with 4 g of [(*n*-C_8H_{17})(C_4H_9)$_3$P]Br.

3.2.4. Effect of hydrogen pressure on the HDS activity. Fig. 11 shows a relatively mild effect of H_2 pressure in the range of 1–7 MPa on the HDS activity of the four types of catalysts coupled with 4 g of [(*n*-C_8H_{17})(C_4H_9)$_3$P]Br at 120 °C with a 4 h reaction time. A higher partial pressure of a gas can lead to its better solubility in liquid medium[54] and hence provides better chances of H_2-catalytic active site interactions. However, at the same time, HDS of DBT results in bulk production of H_2S, which can poison the catalyst and hence inhibit the HDS process at higher pressures.[55–57] The closed autoclave type reactor in this study did not allow the escape of produced H_2S from the reaction system. An increase in H_2 pressure (1 MPa onward) consequently leads to a corresponding increase in H_2S partial pressure, which retarded the HDS process,[56] as shown in Fig. 11. Another reason for the decline in DBT conversion could be the high solubility of H_2S in ILs at higher pressure decreasing the extraction efficiency of the IL.[58] A DBT conversion of 51% by the Pd–Ni–Mo/Al_2O_3 catalyst at 1 MPa H_2 pressure and 120 °C coupled with [(*n*-C_8H_{17})(C_4H_9)$_3$P]Br is superior to an earlier report in terms of catalyst cost, operating pressure and temperature.[18] Based on these results, 1 MPa pressure was selected for onward experiments.

3.2.5. Effect of the amount of IL on the HDS activity of the solid catalyst. The effect of the amount of [(*n*-C_8H_{17})(C_4H_9)$_3$P]Br (3–10 g) using 30 mL of 1000 ppm DBT solution was tested using the optimized reaction conditions. The results compiled in Fig. 12 suggest a corresponding increase in DBT conversion with increasing IL content. A higher IL content provides more sulfur extraction sites and increased H_2 solubility (DFT results in Fig. 8) and hence the maximum DBT conversion (70%) was recorded by the Pd–Ni–Mo/Al_2O_3 catalyst with an oil : IL ratio of 10 : 3.3. These results suggest a 4.5-fold increase in the HDS activity *versus* blank Co–Mo/Al_2O_3 and 2.5-fold *versus* blank Pd–Ni–Mo/Al_2O_3 after coupling with [(*n*-C_8H_{17})(C_4H_9)$_3$P]Br. Furthermore, at 3-fold milder operating conditions than those for the classical HDS process,[59,60] a DBT conversion of 70% with a low-cost (0.5 wt%) Pd-loaded Pd–Ni–Mo/Al_2O_3 catalyst coupled with [(*n*-C_8H_{17})(C_4H_9)$_3$P]Br credits this approach with great promise for industrial applications.

3.2.6. Recycling of IL. The uncontrolled release of used ILs to the ecosystem can concomitantly damage the environment[61] and increases process costs.[62] Thus, [(*n*-C_8H_{17})(C_4H_9)$_3$P]Br was separated and recycled from the HDS products using vacuum distillation and was tested for four consecutive cycles coupled with Pd–Ni–Mo/Al_2O_3 using the optimized conditions. Fig. 13 shows that [(*n*-C_8H_{17})(C_4H_9)$_3$P]Br remained highly stable for four consecutive cycles with net DBT conversions from the first to the last cycle of 70, 68, 68 and 67%, respectively. The Fourier transform infrared (FT-IR) spectra (after four cycles, obtained *via* Nicolet iS50 FT-IR spectrometer) and the ^{1}H NMR (ASCEND-600, Bruker) spectra of the fresh and recycled ILs shown in Fig. S7† revealed minimal changes in the structures of the fresh and recycled ILs. This indicates the highly stable nature of [(*n*-C_8H_{17})(C_4H_9)$_3$P]Br under the current experimental conditions, which could further help in controlling process costs and facilitating the industrial applicability of the proposed process for fuel oil desulfurization.

4. Product analysis and proposed reaction mechanism

Qualitative analyses of the reaction products were performed *via* GC-MS and the chromatograms (pre- and post-HDS reaction) are presented in Fig. S8(a and b).† The DBT peak at the retention time of 14 min was recorded in both the samples.[8] In the post reaction GC-MS chromatogram in Fig. S8b† (performed over Pd–Ni–Mo/Al_2O_3 catalyst at optimized conditions using 10 g of [(*n*-C_8H_{17})(C_4H_9)$_3$P]Br), a new peak for biphenyl (BP) was observed at 9.2 min. This evidenced the preferential direct desulfurization (DDS) pathway for the HDS of DBT.[8,20] This is because at the low temperature of 120 °C, hydrogenation of the benzene ring is not feasible and hence C–S scission occurs preferentially *via* the DDS pathway. In the first step, H_2 attacks the C–S bond, resulting in biphenyl-2-thiol, which is immediately hydrogenated to an unstable hydrogenated BP thiol intermediate, and which upon extraction of H_2S leads to BP. No cyclohexylbenzene (CHB) was found in the product stream (Fig. S8(b)),† which could be due to insufficient catalytic active

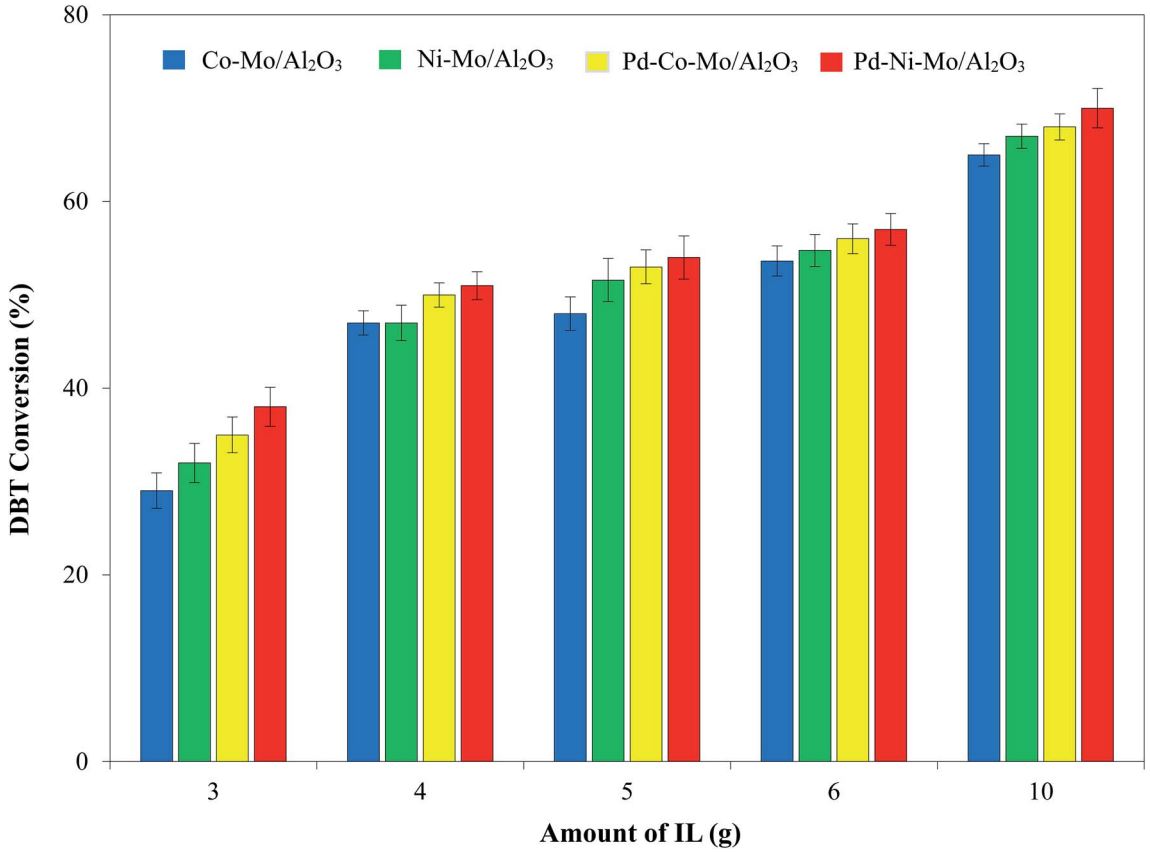

Fig. 12 Effect of amount of IL on DBT conversion using 30 mL of 1000 ppm DBT solution, 1 MPa H_2 pressure, 120 °C reaction temperature, 200 rpm stirring speed and 4 h reaction time.

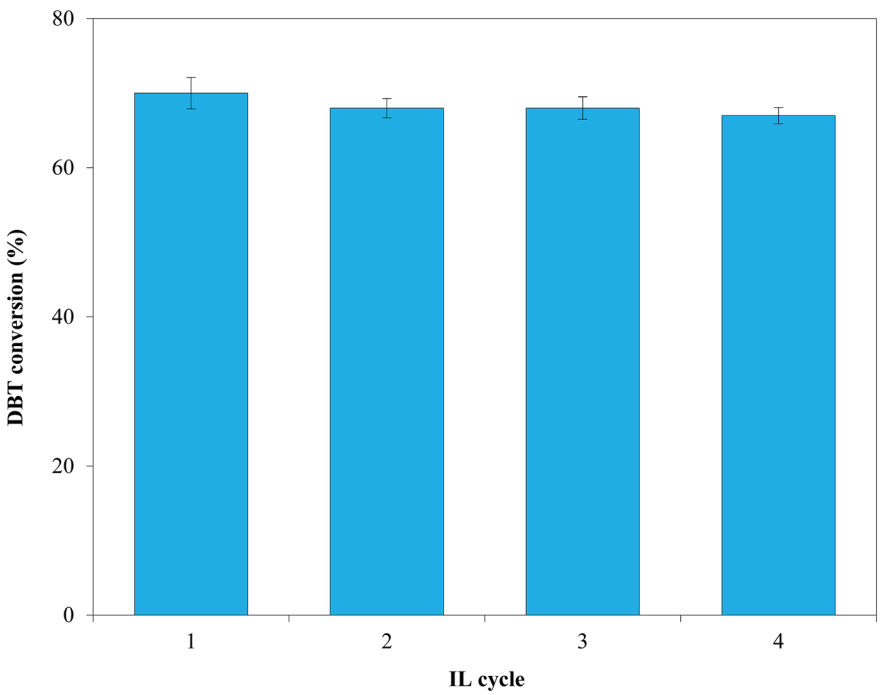

Fig. 13 Effect of four consecutive recycles on DBT conversion using 10 g of $[(n\text{-}C_8H_{17})(C_3H_7)_3P]Br$ coupled with 0.1 g of Pd–Ni–Mo/Al_2O_3 catalyst at 1 MPa H_2 pressure, 120 °C temperature, 4 h reaction time, 200 rpm stirring speed and 30 mL of 1000 ppm DBT solution.

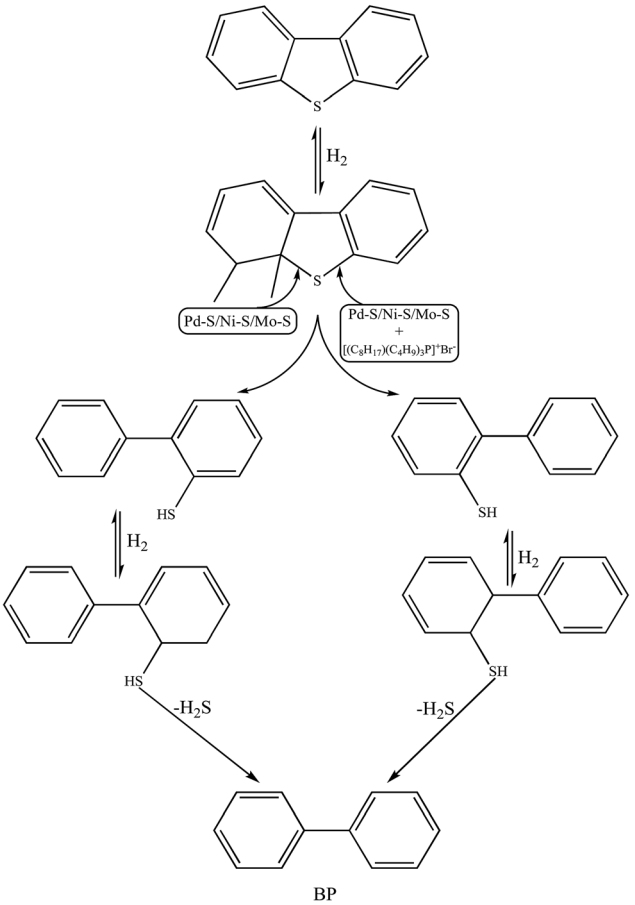

Scheme 1 Proposed reaction mechanism for HDS reaction by blank Pd–Ni–Mo/Al_2O_3 and Pd–Ni–Mo/Al_2O_3 coupled with IL.

sites (having already been used up in the first hydrogenation step of DBT into BP) or engagement of IL with DBT. Another reason could be the mild operating conditions since catalytic hydrogenation of BP into CHB usually occurs at 300 °C and 6.6 MPa H_2 pressure.[63] The reaction mechanism presented in Scheme 1 proposes that the strongly electrophilic Pd active phase in Pd–Ni–Mo/Al_2O_3 readily attacks the electron-rich sulfur center of DBT *via* the DDS pathway, which was further augmented by the synergistic effect of the IL (as DBT extractant)[64] and hence an enhanced DBT conversion (70%) was observed with the coupled application of Pd–Ni–Mo/Al_2O_3 with [(*n*-C_8H_{17})(C_4H_9)$_3$P]Br compared to that for the blank catalyst. From the GC-MS results, it was concluded that the IL merely changed the activity of the HDS process rather than altering the selectivity and chemistry of the HDS reaction.

5. Conclusions

This study reported the integrated application of selected ILs with low Pd (0.5 wt%) loaded Co–Mo/Al_2O_3 and Ni–Mo/Al_2O_3 catalysts in the HDS of DBT under mild operating conditions. The coupled application of ILs synergistically increased the HDS activity of the solid catalysts by about four-fold folds at three times milder operating conditions compared to the conventional HDS process. At genial operating conditions of 1 MPa H_2 pressure, 120 °C temperature, oil : IL ratio of 10 : 3.3 and 4 h reaction time, 70% DBT conversion was achieved over Pd–Ni–Mo/Al_2O_3 coupled with [(*n*-C_8H_{17})(C_4H_9)$_3$P]Br. Textural characterization revealed that Pd incorporation decreased the surface area while increasing the pore diameter of the pristine catalysts. DFT simulations validated that enhanced HDS activity of the solid catalysts coupled with ILs was owing to the synergistic effect of extraction by IL and hydrogenation by the solid catalyst. The IL could be recycled four times with minimal loss of HDS activity. GC-MS results confirmed that the HDS reaction under the current setup followed the DDS pathway. The present approach with its cost-effectiveness (0.5 wt% Pd loading), extremely mild operating conditions with good catalytic activity, and simplified mechanization could be deemed as an alternative approach for the HDS of fuel oils on an industrial level.

Conflicts of interest

The authors declare no conflict of interest.

Acknowledgements

The authors are thankful to the Natural Science Foundation of Guangxi (2017GXNSFDA198047), the Higher Education Commission of Pakistan (Project No: 3365), the Dean Project of Guangxi Key Laboratory of Petro-chemical Resource Processing and Process Intensification Technology (2017Z001 & 2015Z010) and the Postdoctoral Fund of Department of Human Resources and Social Security of Guangxi Zhuang Autonomous Region for the financial support.

References

1 H. Hori, K. Ogi, Y. Fujita, Y. Yasuda, E. Nagashima, Y. Matsuki and K. Nomiya, *Fuel Process. Technol.*, 2018, **179**, 175–183.
2 Y. Muhammad, A. Shoukat, A. U. Rahman, H. U. Rashid and W. Ahmad, *Chin. J. Chem. Eng.*, 2018, **26**(3), 593–600.
3 S. Bhatia and D. K. Sharma, *Biochem. Eng. J.*, 2010, **50**, 104–109.
4 E. Kianpour, S. Azizian, M. Yarie, M. A. Zolfigol and M. Bayat, *Chem. Eng. J.*, 2016, **295**, 500–508.
5 M. J. B. Souza, A. M. Garrido Pedrosa, J. A. Cecilia, A. M. Gil-Mora and E. Rodríguez-Castellón, *Catal. Commun.*, 2015, **69**, 217–222.
6 U. T. Turaga and C. Song, *Catal. Today*, 2003, **86**, 129–140.
7 R. Singh, D. Kunzru and S. Sivakumar, *Catal. Sci. Technol.*, 2016, **6**, 5949–5960.
8 Y. Muhammad, Y. Lu, C. Shen and C. Li, *Energy Convers. Manage.*, 2011, **52**, 1364–1370.
9 W. Shi, L. Zhang, Z. Ni, S. Xia and X. Xiao, *RSC Adv.*, 2014, **4**, 58315–58324.
10 H. Ziaei-Azad and N. Semagina, *Appl. Catal., B*, 2016, **191**, 138–146.
11 Y. Muhammad and C. Li, *Fuel Process. Technol.*, 2011, **92**, 624–630.

12 O. Y. Gutiérrez and T. Klimova, *J. Catal.*, 2011, **281**, 50–62.
13 K. Sakanishi, T. Nagamatsu, I. Mochida and D. D. Whitehurst, *J. Mol. Catal. A: Chem.*, 2000, **155**, 101–109.
14 H. Gao, S. Zeng, X. Liu, Y. Nie, X. Zhang and S. Zhang, *RSC Adv.*, 2015, **5**, 30234–30238.
15 Z. Li, J. Xu, D. Li and C. Li, *RSC Adv.*, 2015, **5**, 15892–15897.
16 A. Arce, M. Francisco and A. Soto, *J. Chem. Thermodyn.*, 2010, **42**, 712–718.
17 P. J. Dyson, D. J. Ellis, T. Welton and D. G. Parker, *Chem. Commun.*, 1999, 25–26.
18 F. Dai, Y. Muhammad, X. Gong, C. Li, Z. Li and S. Zhang, *Fuel*, 2014, **134**, 74–80.
19 R. Navarro, B. Pawelec, J. L. G. Fierro, P. T. Vasudevan, J. F. Cambra, M. B. Guemez and P. L. Arias, *Fuel Process. Technol.*, 1999, **61**, 73–88.
20 R. H. Bowker, M. C. Smith, B. A. Carrillo and M. E. Bussell, *Top. Catal.*, 2012, **55**, 999–1009.
21 M. Yaseen, M. Shakirullah, I. Ahmad, A. U. Rahman, F. U. Rahman, M. Usman and R. Razzaq, *J. Fuel Chem. Technol.*, 2012, **40**, 714–720.
22 A. A. Lemonidou, L. Nalbandian and I. A. Vasalos, *Catal. Today*, 2000, **61**, 333–341.
23 J. A. Cecilia, A. Infantes-Molina, E. Rodríguez-Castellón and A. Jiménez-López, *J. Catal.*, 2009, **263**, 4–15.
24 D. Ferdous, A. K. Dalai and J. Adjaye, *Appl. Catal., A*, 2004, **260**, 153–162.
25 M. S. Rana, E. M. R. Capitaine, C. Leyva and J. Ancheyta, *Fuel*, 2007, **86**, 1254–1262.
26 Y. Huang, Z. Zhou, Y. Qi, X. Li, Z. Cheng and W. Yuan, *Chem. Eng. J.*, 2011, **172**, 444–451.
27 A. M. Venezia, V. L. Parola, B. Pawelec and J. L. G. Fierro, *Appl. Catal., A*, 2004, **264**, 43–51.
28 M. Zhu, Y. Muhammad, P. Hu, B. Wang, Y. Wu, X. Sun, Z. Tong and Z. Zhao, *Appl. Catal., B*, 2018, **232**, 182–193.
29 S. K. Maity, E. Blanco, J. Ancheyta, F. Alonso and H. Fukuyama, *Fuel*, 2012, **100**, 17–23.
30 M. Rezaei, S. M. Alavi, S. Sahebdelfar, P. Bai, X. Liu and Z.-F. Yan, *Appl. Catal., B*, 2008, **77**, 346–354.
31 K. Djebaili, Z. Mekhalif, A. Boumaza and A. Djelloul, *J. Spectrosc.*, 2015, **2015**, 16.
32 K. Zhou, X. Sun, Y. Muhammad, P. Hu, Y. Li, Z. Tong and Z. Zhao, *Appl. Catal., A*, 2018, **555**, 138–147.
33 F.-L. Pua, C. H. Chia, S. Zakari, T. K. Liew, M. A. Yarmo and N. M. Huang, *Sains Malays.*, 2010, **39**, 243–248.
34 K.-K. Liu, W. Zhang, Y.-H. Lee, Y.-C. Lin, M.-T. Chang, C.-Y. Su, C.-S. Chang, H. Li, Y. Shi and H. Zhang, *Nano Lett.*, 2012, **12**, 1538–1544.
35 M. L. Toebes, J. H. Bitter, A. J. van Dillen and K. P. de Jong, *Catal. Today*, 2002, **76**, 33–42.
36 S. J. Sawhill, D. C. Phillips and M. E. Bussell, *J. Catal.*, 2003, **215**, 208–219.
37 J. Iranmahboob, S. D. Gardner, H. Toghiani and D. O. Hill, *J. Colloid Interface Sci.*, 2004, **270**, 123–126.
38 A. Sarkar, A. V. Murugan and A. Manthiram, *J. Phys. Chem. C*, 2008, **112**, 12037–12043.
39 H. W. Wang, P. Skeldon and G. E. Thompson, *Surf. Coat. Technol.*, 1997, **91**, 200–207.
40 C. W. Yi, K. Luo, T. Wei and D. W. Goodman, *J. Phys. Chem. B*, 2005, **109**, 18535–18540.
41 K. K. Sarda, A. Bhandari, K. K. Pant and S. Jain, *Fuel*, 2012, **93**, 86–91.
42 R. Palcheva, L. KaluŽA, A. Spojakina, K. JirÁTovÁ and G. Tyuliev, *Chin. J. Catal.*, 2012, **33**, 952–961.
43 A. Aguirre-Gutiérrez, J. A. M. de la Fuente, J. A. de los Reyes, P. del Angel and A. Vargas, *J. Mol. Catal. A: Chem.*, 2011, **346**, 12–19.
44 Z. Ma, S. H. Overbury and S. Dai, *J. Mol. Catal. A: Chem.*, 2007, **273**, 186–197.
45 S. Zhang, Q. Zhang and Z. C. Zhang, *Ind. Eng. Chem. Res.*, 2004, **43**, 614–622.
46 H. Li, Y. Chang, W. Zhu, W. Jiang, M. Zhang, J. Xia, S. Yin and H. Li, *J. Phys. Chem. B*, 2015, **119**, 5995–6009.
47 F.-t. Li, R.-h. Liu, W. Jin-hua, D.-s. Zhao, Z.-m. Sun and Y. Liu, *Green Chem.*, 2009, **11**, 883–888.
48 W. Jiang, W. Zhu, H. Li, J. Xiong, S. Xun, Z. Zhao and Q. Wang, *RSC Adv.*, 2013, **3**, 2355–2361.
49 C. Song, *Catal. Today*, 2003, **86**, 211–263.
50 O. U. Ahmed, F. S. Mjalli, A. M. Gujarathi, T. Al-Wahaibi, Y. Al-Wahaibi and I. M. AlNashef, *Fluid Phase Equilib.*, 2015, **401**, 102–109.
51 H. Yao, G. Wang, C. Zuo, C. Li, E. Wang and S. Zhang, *Green Chem.*, 2017, **19**, 1692–1700.
52 A. P. Abbott, G. Capper, D. L. Davies, R. K. Rasheed and V. Tambyrajah, *Chem. Commun.*, 2003, 70–71, DOI: 10.1039/B210714G.
53 J. Jacquemin, P. Husson, V. Majer and M. F. Costa Gomes, *J. Solution Chem.*, 2007, **36**, 967–979.
54 R. Luo, X. Zhou, W. Zhang, Z. Liang, J. Jiang and H. Ji, *Green Chem.*, 2014, **16**, 4179–4189.
55 M. S. Rana, J. Ancheyta, P. Rayo and S. K. Maity, *Fuel*, 2007, **86**, 1263–1269.
56 V. Rabarihoela-Rakotovao, S. Brunet, G. Perot and F. Diehl, *Appl. Catal., A*, 2006, **306**, 34–44.
57 M. S. Rana, A. Al-Barood, R. Brouresli, A. W. Al-Hendi and N. Mustafa, *Fuel Process. Technol.*, 2018, **177**, 170–178.
58 Y. J. Heintz, L. Sehabiague, B. I. Morsi, K. L. Jones, D. R. Luebke and H. W. Pennline, *Energy Fuels*, 2009, **23**, 4822–4830.
59 R. Huirache-Acuña, T. A. Zepeda, E. M. Rivera-Muñoz, R. Nava, C. V. Loricera and B. Pawelec, *Fuel*, 2015, **149**, 149–161.
60 S. J. Danforth, D. R. Liyanage, A. Hitihami-Mudiyanselage, B. Ilic, S. L. Brock and M. E. Bussell, *Surf. Sci.*, 2016, **648**, 126–135.
61 T. P. Thuy Pham, C.-W. Cho and Y.-S. Yun, *Water Res.*, 2010, **44**, 352–372.
62 M. Smiglak, J. Pringle, X. Lu, L. Han, S. Zhang, H. Gao, D. MacFarlane and R. Rogers, *Chem. Commun.*, 2014, **50**, 9228–9250.
63 M. Koussathana, D. Vamvouka, H. Economou and X. Verykios, *Appl. Catal.*, 1991, **77**, 283–301.
64 H. Gao, C. Guo, J. Xing, J. Zhao and H. Liu, *Green Chem.*, 2010, **12**, 1220–1224.